Spherulitic Crystallization of Chitosan Oligomers

ARTICLE *in* LANGMUIR · JANUARY 1999

Impact Factor: 4.46 · DOI: 10.1021/la9806754

4 AUTHORS, INCLUDING:

Henri Chanzy

French National Centre for Scientific Research

69 PUBLICATIONS **4,812** CITATIONS

Spherulitic Crystallization of Chitosan Oligomers

Emmanuel Belamie,[†,§] Alain Domard,*[,†] Henri Chanzy,[‡] and Marie-Madeleine Giraud-Guille[§]

Laboratoire d'Etudes des Matériaux Plastiques et des Biomatériaux (UMR CNRS 5627), Université C. Bernard, 43 Bd. du 11 Novembre 1918, 69622 Villeurbanne Cedex, France, CERMAV (CNRS) and Université J. Fourier- BP 53−38041 Grenoble Cedex 9, France, and EPHE, Université P.&M. Curie (URA CNRS 2156), 66650 Banyuls-Sur-Mer, France

Received June 9, 1998. In Final Form: December 1, 1998

Chitosan crystallization, performed by simple drying of an oligomer or polymer solution on a glass or mica surface, was studied at room temperature. Polarizing microscopy revealed the formation of two-dimensional spherulites that were shown to have a negative birefringence. After metal shadowing, electron microscopy investigations allowed the molecular arrangements of these structures to be described more precisely. X-ray and selected area electron diffraction experiments led to the identification of the crystalline structure which corresponds to the monoclinic chitosan hydrochloride. The presence of water in the crystalline lattice was also revealed.

Introduction

The polymorphism of chitosan has been largely studied by different authors, leading to conclusions that largely depend on the conditions of the studies. Chitosan is obtained by heterogeneous deacetylation of chitin and its crystalline structure is therefore derived from that of the initial natural polysaccharide. Clark and Smith[1] were the first to give structural parameters of crystalline chitosan hydrate. Their structure is now widely accepted and was named tendon chitosan by Ogawa et al.[2] Ogawa[3] also showed that heating this initial chitosan at high temperatures leads to the modification of the crystalline structure, and especially the removal of the crystallization water. The anhydrous allomorph obtained under these conditions was named "annealed" chitosan. Ogawa and Inukai[4] and Yamamoto et al.[5] described different crystalline structures obtained by immersing tendon chitosan into highly concentrated acid solutions. In their studies, the molecular arrangement of chitosan and acid was shown to vary with the nature of the acid. Samuels[6] prepared crystalline chitosan films. He described the influence of the preparation process on the structure of these films at both the molecular and macroscopic levels. He reported different polymorphs as well as morphological structures ranging from spherulites to rods. Lamellar crystals with the typical annealed crystalline structure were obtained by Cartier et al.[7] when solutions of short oligomers were precipitated in ammonia under hydrothermal conditions. The precipitation of short oligomers performed by the same authors[8] in concentrated acids led to the formation of crystals having a similar morphology, but a different crystalline structure. The aim of the present work is to investigate the molecular organization of low molecular weight chitosan that was recrystallized at room temperature. Optical and electron microscopic observations were performed to describe the samples from a morphological viewpoint. The crystalline structure and a possible interaction with water were determined by means of X-ray and selected area electron diffraction.

Scheme 1. General Chemical Structure of Chitosan. DA Is the Proportion of Acetylated Repetition Units.

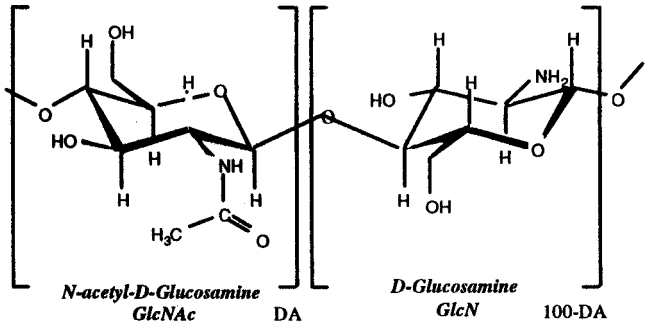

Material and Methods

Initial Material. The initial material, produced from shrimp shells, was a highly deacetylated chitosan kindly provided by Aber Technologies (batch A32E03), with a residual degree of acetylation (DA) near 2%. The extraction, purification, and deacetylation processes were conducted under heterogeneous conditions. The general chemical structure of chitosan is given in Scheme 1.

Preparation of Oligomers. Oligomers were prepared, as described in a previous paper (Belamie et al.[9]), by solid-state hydrolysis of the initial chitosan polymer. Chitosan flakes were first hydrated with the required amount of water to reach a molar ratio of two water molecules per glucosamine residue. They were then inserted into a glass column connected to a bottle of gaseous HCl the flow of which was controlled by a massic debimeter. A wet pH paper positioned at the top of the column became red when reached by HCl, indicating that the column was saturated with HCl and that chitosan, in the amorphous domains, had been converted hydrochloride. The hydrolysis was then obtained

* Address correspondence to A. Domard.
† Université C. Bernard.
‡ CERMAV and Université J. Fourier.
§ Université P.&M. Curie.

(1) Clark, G. L.; Smith, A. F. *J. Phys. Chem.* **1936**, *40* (7), 863.
(2) Ogawa, K.; Hirano, S.; Yui, T.; Watanabe, T. *Macromolecules* **1984**, *17*, 973.
(3) Ogawa, K. *Agric. Biol. Chem.* **1991**, *55*(9), 2375.
(4) Ogawa, K.; Inukai, S. *Carbohydr. Res.* **1987**, *160*, 425.
(5) Yamamoto, A.; Kawada, J.; Yui, T.; Ogawa, K. *Biosci. Biotech. Biochem.* **1997**, *61*, 1230.
(6) Samuels, R. J. *J. Polym. Sci., Polym. Phys. Ed.* **1981**, *19*, 1081.
(7) Cartier, N.; Domard, A.; Chanzy, H. *Int. J. Biol. Macromol.* **1990**, *12*, 289.
(8) Cartier, N.; Mazeau, K.; Domard, A.; Chanzy, H. In *Advances in Chitin and Chitosan*; Brine C. J., Sandford, P. A., Zikakis, J. P., Eds.; Elsevier Applied Science: New York, 1992; p 155.
(9) Belamie, E.; Domard, A.; Giraud-Guille, M.-M. *J. Polym. Sci.* **1997**, *35*, 3181.

10.1021/la9806754 CCC: $18.00
Published on Web 01/28/1999

after 48 h at 65 °C. The acid in excess was eliminated with dry nitrogen and dry air followed by a drying step under reduced pressure at ambient temperature.

Molecular Weight Characterization. The samples were first dissolved then filtered through 0.22 μm pore size membranes (Millipore) before injection into a size exclusion chromatography (SEC) system. The eluent also used as solvent for the samples was a buffer consisting of 0.15 M NH_4OAc to which the required amount of acetic acid was added to reach pH 4.5. The refractive index increment, dn/dc, was 0.172. The separation device comprised a set of two columns: a Waters Protein-Pack 200 SW connected to a TSK-gel G4000 PWXL. A constant flow rate of 0.5 mL·min^{-1} was obtained using an isochratic Spectraphysics pump (Isochrom LC). Injections of 100 μL of filtered solutions at a concentration close to 1% were made by means of an injection loop. A Waters R410 differential refractometer (RI trace) was coupled on line with a Dawn (Wyatt Technologies) multiangle laser light scattering detector (MALLS trace), operated at 632.8 nm.

The average molecular weights of the oligomer samples used in this study were found to be $\bar{M}_n = 2.28 \times 10^4$ g·mol^{-1} and $\bar{M}_w = 4.36 \times 10^4$ g·mol^{-1}.

Optical Polarizing Microscope. A drop of solution in water, at a concentration of 1 wt %, was placed between slide and coverslip and observed with a Leitz Laborlux 12 Pol S optical microscope equipped with crossed polars. A rotating stage allowed us to choose the relative orientation of the preparation with respect to the directions of the crossed nicols. The addition of a λ retardation plate, between the polaroids, allowed the determination of the sign of birefringence within anistropic domains. Micrographs were recorded at magnifications ranging from ×10 to ×40 with the help of an automatic exposure time calculator (Wild MPS 46 Photoautomat).

Replicas Preparation. A drop of oligomer solution at 1% in water was deposited between two pieces of freshly cleaved mica. In some cases, the surface was previously covered with a sputtered carbon layer. These two pieces were then separated and the solution was allowed to dry at room temperature. The sample was then evacuated at 10^{-5} Torr, shadowed with platinum at an elevation angle of 10°, and finally covered with carbon evaporated at 90°. The replicas were then recovered by floating them on bidistilled water and mounting them on electron microscopy copper grids.

Electron Microscopy. Images of the replicas were obtained with a Hitachi 600 electron microscope operated at 75 kV. Analysis and low-dose electron microscopy were performed on a Philips CM200 Cryo electron microscope operated at 200 kV. The samples were introduced either dry or after rehydration overnight at 98% relative humidity (RH) and inserted under frozen hydrated conditions. These samples were observed at liquid nitrogen temperature with the help of a Gatam cold stage sample holder. The calibration of the electron diffraction was obtained with a sample of stretched polyethylene.

X-ray Analysis. A drop of oligomers solution at 1% in water was evaporated under normal temperature conditions on a glass surface. The thin white crystallized layer was then removed by scratching with a razor-blade and the resulting powder was analyzed by X-ray diffraction. The powder was inserted in thin-walled X-ray capillaries of 0.5 mm in diameter. Some capillaries were allowed to dry whereas others were kept overnight at 98% RH and sealed. X-ray powder diagrams were recorded using a vacuum flat film Wahrus X-ray camera mounted on a Philips PW 1720 X-ray generator operated with Cu Kα radiation (λ = 1.5418 Å).

Results and Discussion

Morphological Aspects. *Polarizing Microscopy.* When positioned between partially sealed slide and coverslip, the chitosan solutions were allowed to dry with progressive evaporation of the solvent. Figure 1a shows a typical pattern observed in optical microscopy between crossed nicols, with solutions of chitosan oligomers at concentrations ranging from 1 to 4% (w/v). The edge of the coverslip, i.e., the air interface, is on the left of the micrograph, whereas the inside of the preparation is on the right. In optical microscopy between crossed polars, isotropic domains lack birefringence and remain dark, whereas anisotropic areas appear bright, except for certain positions that depend on the orientation of the index ellipsoid. The first case of extinction occurs when the largest axis of the ellipsoid is parallel to the optical axis, i.e., perpendicular to the preparation plane. The two others are direct consequences of the polarizing technique, because these extinctions occur when the major axis is oriented along the same direction as that of one of the polaroids. At low magnification, the micrograph in Figure 1a shows large domains, mainly inside the preparation, that remain dark and correspond to amorphous zones, as confirmed when the microscope stage is rotated around its optical axis. Birefringent domains nucleate and grow between slide and coverslip near the air interface. On the right side of the photograph, they have the form of small rodlike or fan-shaped elements, depending on their stage of growth and their orientation with respect to the axes of the polaroids. Near the air interface these elements are disklike and often fuse to form a mosaic of bright domains separated by sinuous extinction lines. At higher magnification, the small spherulite (A) presented in Figures 1b

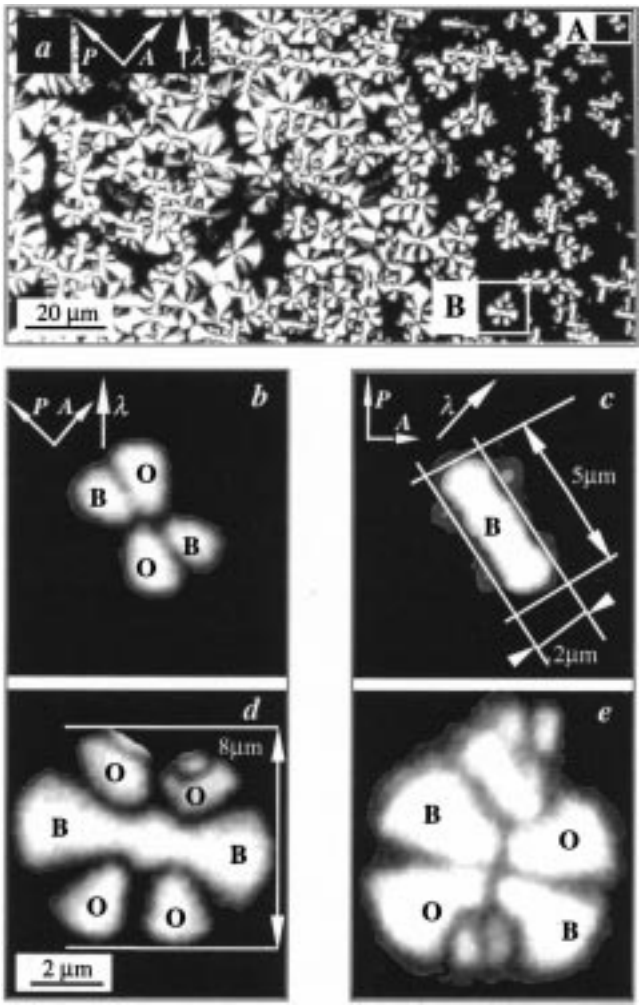

Figure 1. (a) Spherulites grown from a solution of chitosan oligomers at 1% and observed by optical microscopy in polarized light between cross polaroids. The air interface is located on the left of the micrograph. (b−e) Enlarged views of the two germs A and B present in Figure 1a, with two extreme orientations of the polaroids. The polaroid orientations are given in Figure 1b for (b) and (d), and in Figure 1c for (c) and (e). The color indications (O, orange; B, blue) are relative to observations made after introduction of a λ retardation plate.

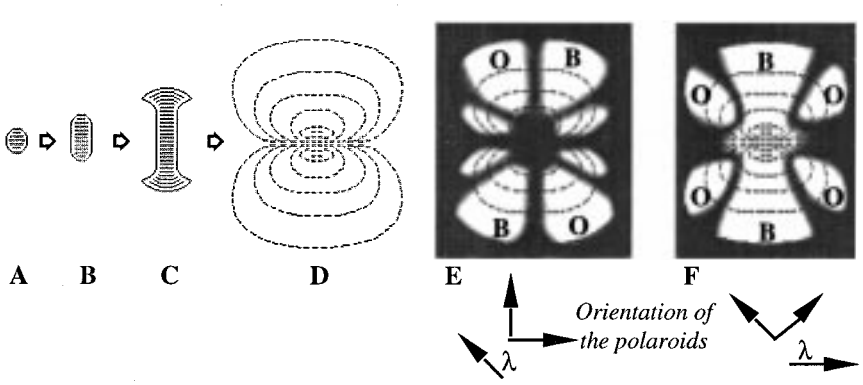

Figure 2. Schematic representation of the growing process of a spherulitic germ from the nucleus stage (A) to the final spherulite (D) from Keller (1955). E and F are representations of the theoretical patterns that should be observed with such crystals when seen in polarized light between cross polaroids. The color indications are those that are supposed to be observed by introducing a λ retardation plate, with (O) orange and (B) blue.

and c appears to change shape when the microscope stage is rotated. It presents a circular birefringent area and a typical dark maltese cross with arms parallel to the direction of the polaroids in one orientation (Figure 1b). A 45° rotation leads to a rod shape with four small bright disks arranged symmetrically at both ends faintly visible in Figure 1c. Larger spherulites exhibit more complicated patterns that are characteristic of a spherulitic organization observed between crossed polars. These patterns depend on the stage orientation with respect to the polaroids, as illustrated in Figures 1d and e, which correspond to extreme situations. All of these patterns are typical of a spherulitic crystallization. The different elements that we have observed and described here correspond to different steps of crystalline growth. We propose that chitosan oligomers follow the model of spherulite growth proposed by Keller[10] and presented in Figure 2. In this model, the growing sequence starts with a small spherical seed (Figure 2a). Its development on opposite sides leads to a rectangular outline (Figure 2b), and then to the formation of fans at both ends, giving a dumb-bell like shape (Figure 2c). The complete development of the fans causes the final structure to be almost spherical or disklike. In our case, during evaporation of the solvent, a crystalline seed can arise from the solution, and depending on different conditions that we shall discuss further, the seed can more or less develop and form either individual rodlike structures or a mosaic of connected spherulites. Figures 3a and b display two different situations often observed. In both cases, the patterns are a consequence of the impingement of spherulites during their growth that leads to the formation of a mosaic. In the first case (Figure 3a), the concentration is about 1% (w/v). The resulting spherulites are large, with a diameter of the order of 10 μm. The typical appearance of spherulites observed in polarized light is still visible. Conversely, the pattern presented on Figure 3b no longer exhibits an obvious spherulitic character, but a complicated texture appears with bright domains separated by sinuous extinction lines and dark regions. These dark zones do not become bright when the stage is rotated. In contrast, the extinction lines move inside the bright regions when the stage is rotated. Nevertheless, the response obtained in that case can be related to the formation of a mosaic of very small connected spherulites. In addition, it is likely that extensive spherulite superimposition can occur as a result of the rather large initial concentration; 4% in that case. The subsequent addition or subtraction of optical path difference in the width of the preparation could thus

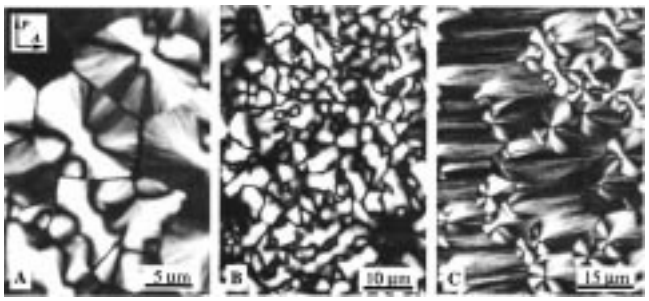

Figure 3. Different situations often observed in polarized light between cross polars. (A) Mosaic of large connected spherulites. (B) Mosaic of small connected and/or superimposed spherulites. (C) "Comet" spherulites observed near the edge of the coverslip.

explain the complexity of the patterns. Such patterns have been described with polyethylene adipate, for instance, by Mandelkern.[11] Another type of pattern, namely asymmetric spherulites, was observed with some preparations, and is presented in Figure 3c. Such a situation occurs when the preparation is not sealed, allowing a fast evaporation of the solvent. This type of crystallization has been described for other polymers, such as acetal (Saville[12]) in particular conditions of crystal formation. Acetal crystals were grown from the melt by cooling and Saville shows how elongated spherulites are a result of a faster cooling of the outside of the sample. In our case, the crystals do not arise from the melt but the reasoning remains the same because these spherulites are found near the air interface, where evaporation of the solvent is faster. In such a situation, it is likely that the crystal growing rate becomes much faster than the germination rate. The spherulites can thus develop over long distances in one preferential direction, which is determined by the presence of numerous nuclei aligned close to one another at the air interface. The introduction of a first-order retardation plate (λ) gives the kind of patterns schematically reproduced in Figures 2e and f. When the largest axis of the index ellipsoid is lying parallel to the vibration direction of λ, the color of the zone changes from the first-order white to blue. Conversely, when they are lying perpendicular, the color of the quadrant is moved toward orange. In our case, according to the observed patterns, we can conclude that the spherulites have their larger refractive index in the tangential direction and thus have a negative birefringence. This is consistent with the

(10) Keller, A. *J. Polym. Sci.* **1955**, *17*, 447.

(11) Mandelkern, L. In *Crystallization of Polymers*; Mc-Graw-Hill Book Company, New York, 1969.

(12) Saville, B. P. In *Applied Polymer Light Microscopy*; Hemsley, D. A., Ed.; Elsevier Applied Science: London, 1989; p 111.

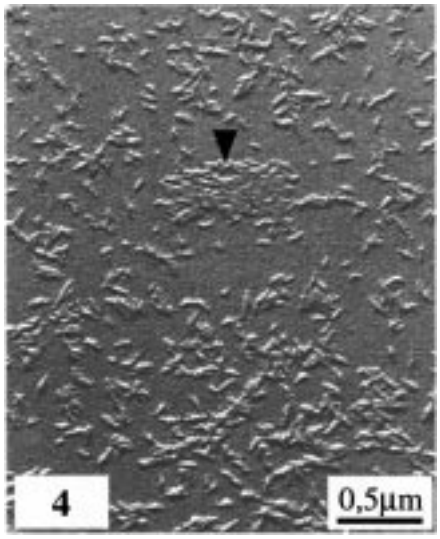

Figure 4. Individual rodlike units of about 20 nm in width, and a bundle (black arrowhead). Figures 4−9 are electron micrographs recorded with platinum shadowed samples prepared by drying a drop chitosan oligomers solution on a mica surface. Each of them displays different steps of crystal growth.

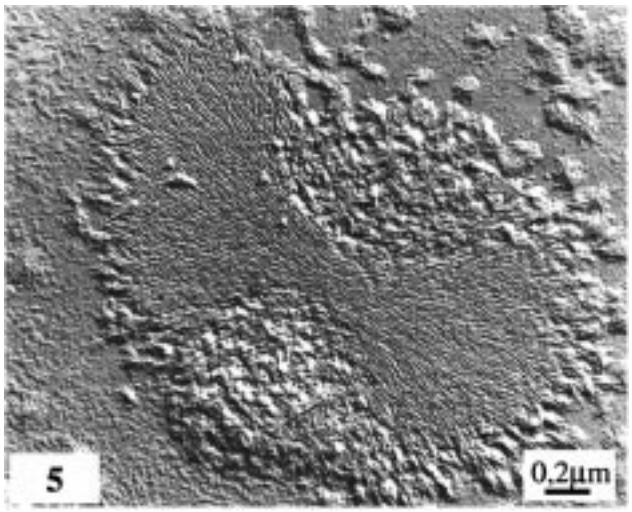

Figure 5. The dumb-bell shape of the spherulite is typical of early stages of growth.

growing sequence presented on Figure 2 and with the molecular orientation proposed for the final spherulite (Figure 2d).

Electron Microscopy. Samples were prepared as described in the Materials and Methods and observed in transmission electron microscopy (TEM) after platinum shadowing. We observed different situations that could correspond to different growth stages of the spherulites. Figure 4 shows small rodlike individual particles of about 20 nm in width with no particular orientation in the field of view. Some bundles are visible (black arrowhead) but the particles are quite well dispersed. Figure 5 shows a large striated structure with a central rodlike domain with fan-shaped extensions on both sides. The striations are parallel to the long axis of the central part and fan out to the edges of the growing spherulite, in such a way that they run perpendicular to the border. In the free space left between the fans on both lateral sides of the central part, one can observe the presence of some granular material, exhibiting no particular orientation and no striation. The same kind of granular material is visible

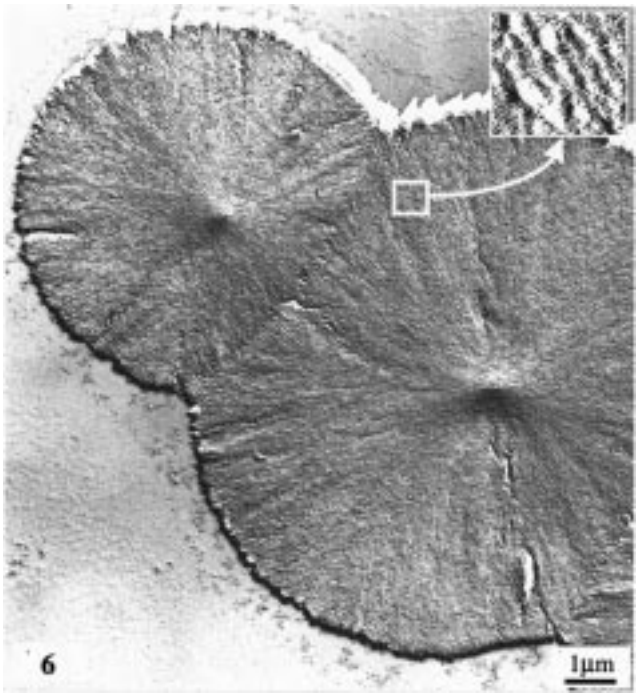

Figure 6. Two connected spherulites. The inset is a enlarged view of the region squared showing the secondary striation.

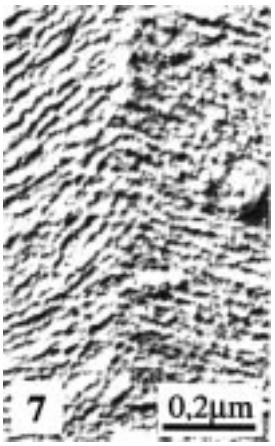

Figure 7. Enlarged view of a junction zone.

near the edges of the fans. This kind of polycrystalline assembly in the form of a dumb-bell is known to be an early stage of spherulites growth. The central body, which exhibits an almost rectangular outline, acts as a starting point for the development of the whole circular structure. Figure 6 shows connected spherulites, each having a quite circular shape with diameters ranging from about 5 to 10 μm. In some cases, we obtained individual spherulites with a very regular outline (not shown). In the present situation, the two spherulites met one another on one of their growing sides during their development. Depending on the situation, the boundary line can either be a straight line or a curve. This impingement zone is seen at higher magnification in Figure 7, in which one can observe the interpenetration of two neighboring spherulites. In some other cases, a gap can appear between two spherulites as shown in Figure 8. Here, the space between the two structures appears devoid of organized matter. It has to be specified that the spherulites I and II (as marked in Figure 8) were normally developed, except in this region. In the literature of synthetic polymers, it has been postulated that some noncrystallizable material could

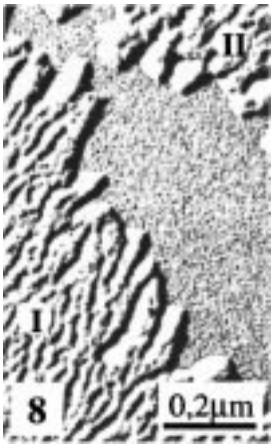

Figure 8. Enlarged view of a gap between two spherulites.

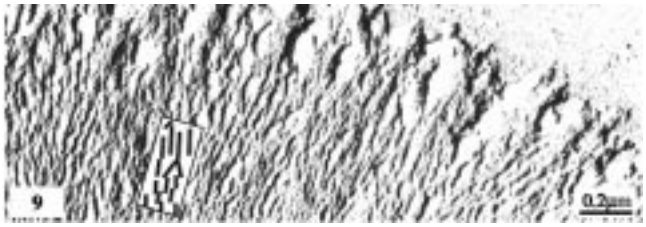

Figure 9. An electron micrograph taken at the top of a fan of a spherulite after platinum shadowing. The variations of the orientation of the monocrystals are schematically shown in the rectangular box, the orientation of which corresponds to that of the average radius.

accumulate near the growing front.[13] For this reason, when two growing faces become close enough, the growing rate can be considerably lower. This could probably explain why a gap can take place between two spherulites, instead of an impingement zone. On the spherulites presented in Figure 6, the radial striation is still present except on both sides of the central part, between the fans. When looking carefully to the ridges, one should observe that their orientation is not always exactly parallel to the radius but the ridges often make a small angle around this direction. This is particularly visible in the micrograph in Figure 9 that was taken at the top edge of a spherulite. In addition, the shadow obtained after metalization gives a thickness of the spherulite comprised between 20 and 30 nm. When this value is compared to the average radius (10−15 μm), it clearly appears that the structure is essentially flat, and thus that crystallization was mainly two-dimensional. In addition to these well-formed circular spherulites, we have observed also the presence of "exotic" spherulites (not shown) that exhibit an asymmetrical structure, a consequence of a faster growth on one particular side of the nucleus. It is likely that these asymmetric spherulites are of the same type as the elongated spherulites we observed in polarizing microscopy. We thus propose that they nucleated near the edge of the drop, close to the air interface. The small individual nuclei are likely formed by a lateral aggregation of oligomer chains leading to a rodlike morphology, growing perpendicular to the chain direction in a typical polymer single crystal fashion. In this scheme, the single nucleus grows in the form of a fibril that repeatedly branches during further growth, so as to fill up the space available. In many other crystalline forms, the nucleus gives rise to a single crystal with all the molecules having the same three-dimensional orientation. In the case of spherulites, the branch and the parent crystallite make a certain angle, independent of their crystalline structure. Although the branching is thus said to be noncrystallographic, the major axis of the crystallites remains more or less parallel to the radii of the whole spherulite. This peculiar crystallization process is clearly identified on the different electron micrographs, especially in Figure 9, where it can be seen that the crystallites orientation oscillates around that of the spherulite radius. Note also that the ridges, when observed at a higher magnification (inset in Figure 9), exhibit a secondary striation approximately perpendicular to the main axis of each elemental unit forming the primary striation. Most of the situations encountered on replicas in TEM can be related to patterns observed in polarized light. For example, the dumb-bell like structure in Figure 5 corresponds to the birefringent elements in Figures 1b and c when viewed in polarized light for two extreme positions of the polaroids. The mosaics of large connected spherulites are also identified in light microscopy as shown in Figure 3a, as well as the elongated spherulites presented in Figure 3c.

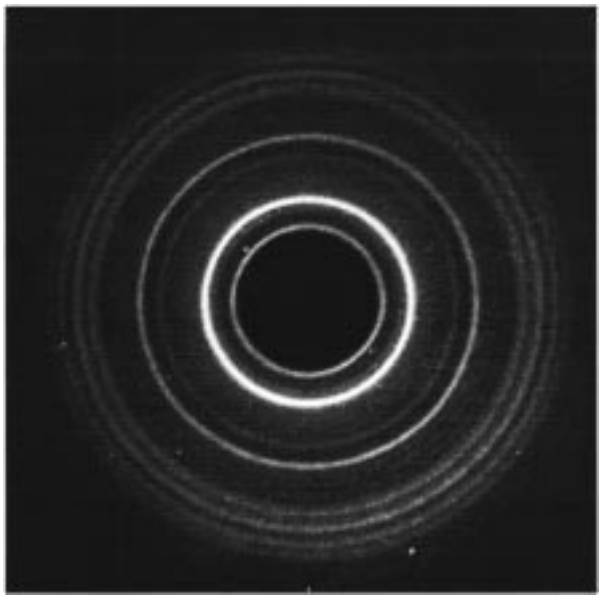

Figure 10. The X-ray diffraction powder pattern obtained with a hydrated sample in the hydrochloric form.

Crystallographic Aspects. *X-ray Diffraction Analysis.* When X-ray powder diffraction diagrams were recorded on dry spherulite specimens, poorly resolved diagrams (not shown) containing only two broad rings were obtained. On the other hand, when the samples were kept under hydrated environment, well-resolved X-ray patterns could be recorded. An example of hydrated pattern is shown in Figure 10. This diagram, which extends to a resolution of around 0.3 nm, displays a series of sharp diffraction rings. A list of the measurable reflections and their *d*-spacings is presented in Table 1. As expected, this powder diagram is in complete agreement with the X-ray fiber pattern of chitosan hydrochloride described by Ogawa and Inukai.[4] It is also nearly the same as the hydrated X-ray powder pattern resulting from a preparation of single crystals of chitosan prepared in aqueous HCl (Cartier et al.[8]). The listing of the reflections of our patterns is presented in Table 1 together with the data set reported by Cartier et al.[8] and its correspondence with that of Ogawa and Inukai.[4] In Table 1 is also presented the indexation proposed by these authors who have refined their X-ray analysis in terms of a monoclinic structure with $a = 1.381$ nm, $b =$

(13) Wunderlich, B. In *Macromolecular Physics*; Academic Press: New York, 1976.

Table 1. *d*-Spacings, Relative Intensities, and Possible Indexation of the Diffraction Rings in the X-ray Powder Diagrams of Hydrated Chitosan Hydrochloride Spherulites

ring number	*d*-spacings (nm) (this work)[a]	*d*-spacings (nm) (Cartier[8])[a]	*d*-spacings (nm) (Ogawa and Inukai[4])[a]	indexation monoclinic[b]	tetragonal[c]
1	1.083 (s)	1.090 (s)	1.069 (vs)	$1\bar{1}1$	111
2	0.854 (w)		0.853 (s)	$1\bar{1}3$	113
3	0.776 (vs)	0.785 (vs)	0.787 (vs)	$0\bar{2}0$, 120	020, 200
4	0.555 (m)	0.555 (w)	0.553 (s)	$2\bar{2}0$, 030	220, 221
5	0.492 (vs)	0.493 (s)	0.491 (vs)	$22\bar{1}$, 131	311, 131
6	0.391 (m)	0.396 (m)	0.389 (m)	$1\bar{4}1$	041, 401, 040, 400
7	0.371 (m)	0.370 (m)	0.366 (s)	$3\bar{3}1$, $2\bar{4}1$	331
8	0.349 (m)	0.353 (m)	0.347 (m)	$4\bar{1}0$, 400	420, 240

[a] vs: very strong, s: strong, m: medium, w: weak. [b] Indexation following the monoclinic unit cell of Ogawa and Inukai[4] with unit cell parameters $a = 1.381$ nm, $b = 1.633$ nm, $c = 4.073$ nm, $\gamma = 96.46°$. [c] Indexation following the alternative tetragonal unit cell with cell parameters $a = b = 1.574$ nm and $c = 4.073$ nm.

1.633 nm, c (chain axis) = 4.073 nm, and $\gamma = 96.46°$. The pattern in Figure 10 could also be indexed either as a tetragonal or orthorhombic pattern with unit cell parameters $a = b = 1.574$ nm and $c = 4.073$ nm. Ogawa and Inukai,[4] who noticed also a possible 4-fold symmetry around the fiber axis of these samples, also considered the tetragonal indexation which is listed in Table 1. Despite this possibility, these authors nevertheless preferred a monoclinic symmetry on the basis of stereochemical considerations. Note that despite a difference in their preparation, our chitosan hydrochloride spherulites gave the same diffraction diagrams as those of Ogawa and Inukai.[4] In their work, these authors started from hydrated chitosan tendon fibers which were immersed for 10 min in 6 N HCl before being washed. Thus, their conversion was essentially achieved by a solid-state complexation of chitosan with acid and water. In our case, as well as that of Cartier et al.,[8] the specimens resulted from a direct crystallization from aqueous acid solution. From the present results, we can conclude that all of these techniques gave the same type of crystalline chitosan hydrochloride product. In all cases, the structures contained a substantial amount of intracrystalline water molecules that need to be kept in order to preserve the crystalline nature of the system.

Electron Diffraction Analysis. The thinnest two-dimensional chitosan spherulites could also be investigated by TEM in imaging and electron diffraction modes. When achieved under frozen hydrated conditions (Chanzy et al.[14]), the resulting electron diffraction diagrams consisted of arrays of spots that revealed the orientation of the crystalline domains within the spherulites. A typical electron diffraction pattern and its corresponding image are shown in Figure 11. The diagram which was recorded on about 0.2 μm^2 of the specimen contains 30 spots symmetrically mirrored along the four quadrants. The indexation and calibration of this diagram and its comparison with the X-ray data of Ogawa and Inukai[4] together with the X-ray and electron diffraction of Cartier et al.[8] indicate that the pattern can be indexed along the $hk0$ and $hk1$ Miller indices of hydrated chitosan hydrochloride. Thus, in the corresponding diffracting crystals, the chitosan chains are essentially perpendicular to the plane of the thin spherulites. The pattern in Figure 11 corresponds very closely to that of a single crystal of this product recorded by Cartier et al.[8] Our diagram, as well as that of Cartier et al.,[8] is highly symmetrical and does not present any hint of monoclinic character. The diagram in Figure 11 is indexed along the two vectors shown in the figure. Both vectors have the same lengths and are oriented respectively along the spherulite radius and perpendicular to it. The tetragonal indexation of the diagram containing at the same time $hk0$ and $hk1$ diffraction spots is presented in Table 2. In Figure 11, there are at the same time diffraction spots that can be indexed as $hk0$ and $hk1$. This occurrence is classical, with electron diffraction of thin plateletlike objects when the unit cell parameter perpendicular to the platelet base is large. Indeed, the reciprocal diffraction spots of such objects consist of spikes, elongated perpendicular to the platelet plane (Hirsch et al.[15]). Because the c cell parameter is fairly large, its reciprocal c^* is quite small and therefore the layers of reciprocal spots perpendicular to c^* are very close to one another. For this reason, the spiky reciprocal spots of the first layer

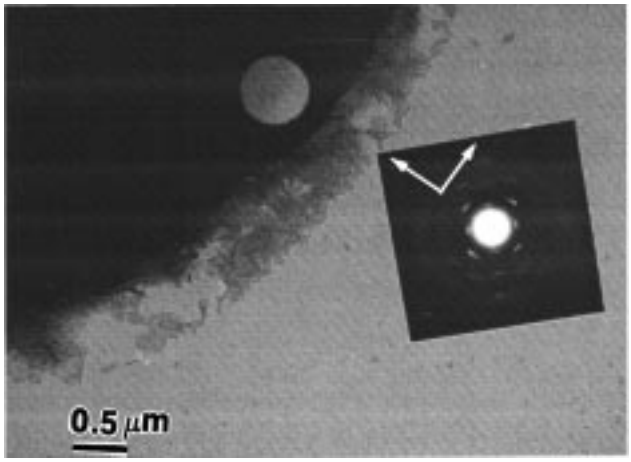

Figure 11. Low-dose electron micrograph recorded with a frozen hydrated specimen. Inset: electron diffraction diagram corresponding to the circled area and printed with the proper orientation with respect to the image.

Table 2. *d*-Spacings, Intensities, and Probable Indexation of the Electron Diffraction Data Recorded on Thin Frozen Hydrated Chitosan Hydrochloride Spherulites

spot[a]	*d*-spacings (nm)	intensity	indexation[b]
1	1.073	s	111
2	0.793	vs	020, 200
3	0.552	m	220, 221
4	0.506	m	130, 310, 131, 311
5	0.393	m	040, 400, 041, 401
6	0.385	m	330, 331

[a] Only the spots occurring in one quadrant are considered. [b] Indexation following the tetragonal unit cell with cell parameters $a = b = 1.574$ nm, $c = 4.073$ nm. The indexation along $hk1$ is in correlation with the X-ray fiber pattern recorded by Ogawa and Inukai.[4]

(14) Chanzy, H.; Guizard, C.; Vuong, R. *J. Microsc.* **1977**, *111*, pt 1, 143.

(15) Hirsch, P. B.; Howie, A.; Nicholson, R. B.; Pasheley, D. W. In *Electron Microscopy of Thin Crystals*; Butterworth: London, 1965.

will intersect the Ewald sphere of diffraction. In the present case, because the electron diffraction diagrams were recorded at an accelerating voltage of 200 kV, the Ewald sphere is so large that it can be assimilated to the base plane. Thus, all the strong *hk*1 diffraction spots are expected to be seen among the *hk*0 spots in the base plane. This is the case in particular for the strong 111 at 1.073 nm, together with the 131 and 311 at 0.506 nm. Another reason for the presence of higher layer line diffraction spots in the diagram shown in Figure 11 may be connected with the occurrence of a twisting of the crystals along the radius of the spherulite. Indeed, this type of twisting is quite common with polymer spherulite (Keller[10]). If it could be confirmed in the present study, it could explain also the negative birefringence of the spherulites. This optical property indicates that there are some chitosan chains that are located in the plane of the spherulite and directed with their axes perpendicular to the spherulite radius. Such a situation is likely to occur if the crystals of chitosan are indeed twisted along the spherulite axis. Thus, the electron diffraction would correspond only to crystals that are oriented with their chain axis perpendicular to the plane of the thin spherulites. Conversely, the observed specific birefringence would result from the crystals where the chains are in the plane of the spherulites.

Conclusions

In this study we demonstrated that chitosan oligomers were able to crystallize in the form of spherulites. These polycrystalline structures were described either in optical microscopy in polarized light or by electron microscopy after metal shadowing. The observations made with both techniques gave consistent data about the morphology of the structures. Optical microscopy gave us some information about the birefringence of the structures, whereas electron microscopy gave some data at the molecular level. The spherulitic behavior is widely observed in the field of natural and synthetic polymers. We can mention for instance spherulitic dextran or cellulose in the field of polysaccharides, and polyethylene for synthetic polymers. In both cases, as in many others, a great number of studies have been carried out that led to the quite complete understanding of either the crystallization process or the molecular organization. It seems that low molecular weight chitosan oligomers behave almost like several polymers, at least in the conditions of our study.

We have shown by electron diffraction that the chitosan chains are essentially perpendicular to the plane of the spherulites. However, the birefringence observed in polarized light lets us suppose that the largest index is parallel to the plane of observation, and is thus parallel to the plane of the spherulites. In addition, this index is arranged in a concentric way, meaning a negative birefringence of the whole structure. It is thus likely that, because of a twisting of the monocrystals, the chitosan chains take different orientations within the structure. For this reason, and despite the 4-fold symmetry of the tetragonal lattice, one can observe on the same samples, either birefringence or electron diffraction.

A lot of chitosan polymorphs have been described, depending on a number of parameters among which the most influent are the saline form, the temperature of crystallization, and the pH. In our case, the crystals were grown at room temperature, the molecules being oligomers in the hydrochloric form. In addition, we have shown, either by X-ray diffraction or electron diffraction, that water molecules are probably inserted in the crystal lattice. This is different from results obtained, for example, by Cartier et al.,[7] and in general for high-temperature polymorphs (Mazeau et al.;[16] Yui et al.[17,18]), for which no difference was observed between diffraction patterns obtained either with hydrated or anhydrous crystals. We demonstrated that the allomorph we observed in this study is the same as that described either by Cartier et al.,[8] Ogawa and Inukai,[4] or Yamamoto et al.[5] despite very different preparation pathways.

Acknowledgment. We thank Y. Bouligand for fruitful discussions about molecular ordering and his help in the interpretation of the polarized light microscopy observations.

LA9806754

(16) Mazeau, K.; Winter, W. T.; Chanzy, H. *Macromolecules* **1994**, *27*, 7606.

(17) Yui, T.; Imada, K.; Okuyama, K.; Obata, Y.; Suzuki, K.; Ogawa, K. *Macromolecules* **1994**, *27*, 7601.

(18) Yui, T.; Ogasawara, T.; Ogawa, K. *Macromolecules* **1995**, *28*, 7957.